APL Photonics

Investigation of UV filaments and their applications

Cite as: APL Photonics **6**, 060803 (2021); https://doi.org/10.1063/5.0050579
Submitted: 16 March 2021 • Accepted: 25 May 2021 • Published Online: 11 June 2021

Ali Rastegari and Jean-Claude Diels

Investigation of UV filaments and their applications

Cite as: APL Photon. 6, 060803 (2021); doi: 10.1063/5.0050579
Submitted: 16 March 2021 • Accepted: 25 May 2021 •
Published Online: 11 June 2021

Ali Rastegari and Jean-Claude Diels[a)]

AFFILIATIONS

Center for High Technology Materials, University of New Mexico, Albuquerque, New Mexico 87106, USA

[a)]Author to whom correspondence should be addressed: jcdiels@unm.edu

ABSTRACT

UV laser pulses at 266 nm with 170 ps duration and up to 300 mJ energy create UV filaments. The effects of different beam preparation scenarios on UV filamentation are discussed. Beam preparation by focusing in vacuum and launching into the atmosphere through an aerodynamic window establishes the existence of filaments as self-guided non-diffracting entities. In addition, focusing through the aerodynamic window converts the initial super-Gaussian into a parabolic beam profile at the edge of the nonlinear medium (air). The shock-wave generated by the UV filament is investigated via shadowgraphy techniques. The shock-wave is cylindrically symmetric, leaving a low density channel behind, which is well-sustained for 1 ms, as it propagates outward. This low density channel is a waveguide that can be used for guiding purposes. Applications of UV filaments including guiding, remote sensing, and drag reduction for supersonic aircrafts are discussed.

I. INTRODUCTION

Laser filamentation is a phenomenon that has attracted much attention in the past few decades and has many applications, including remote sensing,[1–3] laser guided electrical discharges,[4–8] and air lasing.[9–13] Filamentation was defined by Akhmanov[14] as a self-guiding phenomenon that can occur in transparent media with an intensity-dependent index of refraction. If the non-linearity of the medium is positive at moderate intensities (self-focusing) and saturates or turns over (self-defocusing) at higher intensity, a stable waveguide can be formed, which can exist for distances exceeding the Rayleigh range. Such stable waveguides were observed in liquids at very low optical powers, exploiting the nonlinearity of micro-emulsions.[15] One requirement for observing nonlinear collapse and filamentation is that the beam power exceeds the critical power for self-focusing.[16,17] The power required in air being in excess of 12 GW at 800 nm, atmospheric filamentation was first demonstrated with femtosecond pulses of several mJ energy from amplified Ti:sapphire lasers.[18] Since the critical power for self-focusing is much lower in the UV (13 MW at 250 nm),[19] filamentation in air was also observed with sub-mJ ps pulses at 248 nm.[20] Another requirement for filamentation is that the pulse duration be shorter than the time required to heat the photo-excited electrons by inverse bremsstrahlung to the ionization potential. This time being in the ns range at 250 nm and in the ps range at 800 nm makes it possible to carry much higher energies in UV filaments than in IR filaments.[21] For the same amount of loss, the larger reservoir of energy in the shorter wavelength pulse will take longer distances to be depleted by losses. The length of a single near-infrared (NIR) filament is mainly limited by nonlinear losses (for instance, generation of conical emission). In the case of less intense UV filaments, a loss of 60 μJ/m was measured,[21] which is a very small fraction of tens of mJ energy of the 170 ps UV pulse.

II. LASER SOURCE

The UV laser source is briefly introduced in this section. Different beam preparation techniques leading to different types of filamentation are presented in Sec. III. Measurement of beam profiles presented in Sec. IV involves either high power linear attenuators, shadowgraphy, or impact measurements.

Most ultrashort/intense laser pulse sources start from an oscillator generating fs pulses that are subsequently stretched to ps for amplification. In an effort to create a more robust laser source, we start with a Q-switched ns oscillator–amplifier Nd:YAG system, a workhorse of the laser industry. A Q-switched injected–seeded Nd:YAG oscillator generates a single longitudinal mode, 10 ns pulses with a repetition rate of 1.25 Hz.[22] After amplification through a six-stage single-pass Nd:YAG amplifiers, the energy of the 1064 nm

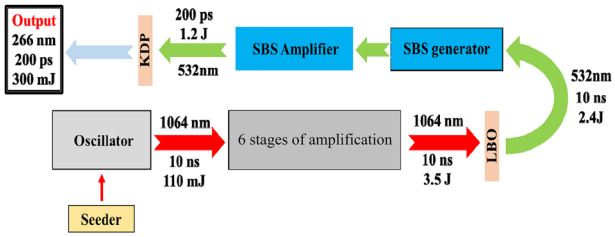

FIG. 1. Schematic diagram of the UV laser.

pulses increases up to about 3.5 J and is frequency doubled to 532 nm through a LBO crystal (Cristal Laser, France).[23] The 532 nm pulses with an energy of up to 2.4 J are compressed by stimulated Brillouin backscattering in two water cells arranged in an oscillator–amplifier configuration.[24,25] The phonon lifetime limit of water at 532 nm is about τ_{ph} = 295 ps. With a 10 ns input pulse of 300 mJ energy, a minimum compressed pulse duration of 180 ps ($0.6\tau_{ph}$) and output energy of 240 ps (at 532 nm) in a SBS amplifier cell. Details can be found in Ref. 25. The compressed green pulses are thereafter frequency doubled in a KDP crystal, with an efficiency limited to only 10 to 20% by two-photon absorption. The resulting pulses at 266 nm are 170 ps in duration and 300 mJ energy[26] (Fig. 1).

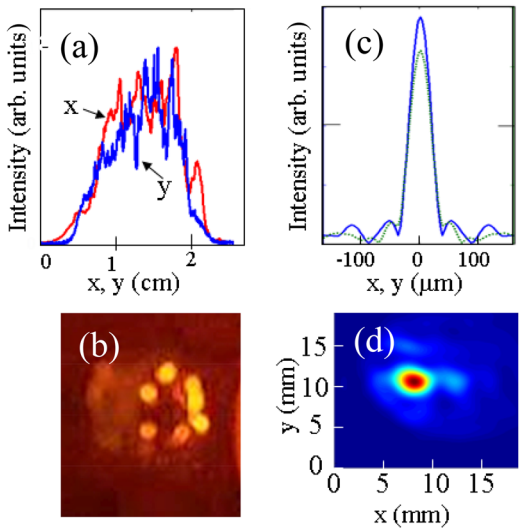

FIG. 2. (a) Profile of the super-Gaussian 266 nm beam. (b) Filament pattern produced by the profile (a) in air (aerodynamic window is not operational). (c) Far field profile as produced in vacuum with the operational aerodynamic window (hence, in the absence of nonlinear effect) at the focus of a lens. (d) Single filament profile taken at 2 m from the exit of the aerodynamic window.

III. BEAM PREPARATION

A. Introduction

For the purpose of filamentation, the source presented in Sec. II presents two major challenges. First, the unstable cavity of the oscillator creates a super-Gaussian beam profile. Second, the spatiotemporal profile of the beam resulting from the oscillator and amplifier has a curved energy profile. The latter results in an undesirable energy spread along the propagation direction in a focused beam.

The super-Gaussian profile is ideal for obtaining high energy from the oscillator and amplifiers, as well as for harmonic generation. It is well known, however, that such a beam results in the formation of multiple filaments distributed along a circle.[27] This filament configuration remains the same for all focusing geometry because the nonlinear lensing dominates before the far field pattern from diffraction is achieved.

A typical profile of the 266 nm beam is shown in Fig. 2(a). Figure 2(b) shows the circle of filaments created by this flat-top profile. If focused in vacuum, in the absence of nonlinearity, the beam profile will be the Fraunhofer diffraction of the super-Gaussian shown in Fig. 2(c). This far field diffraction having a parabolic profile on axis is favorable for the formation of a single filament, as shown in Fig. 2(d). The challenge here is not to focus the beam in vacuum, but to launch the focused spot in air through a window that can withstand the high intensity of the beam. It is shown in Subsection III B that an "air window" can be created in the expansion chamber of a supersonic nozzle. Another property of this window is that it does not introduce beam pointing instabilities and turbulence that would perturb the nonlinear focusing, defocusing, and guiding.

The purpose of using a focused beam in vacuum as the initial condition is twofold. First, it serves as eliminating high spatial frequencies prior to entering the nonlinear medium. Second, it serves to establish the existence of filaments as self-guided non-diffracting entities, as opposed to a moving focus. The latter phenomenon relates to damage tracks produced in transparent solids by intense nanosecond pulses.[28] As the pulse power increases beyond the critical power along the leading edge of the pulse, the self-focus recedes from infinity to the shortest distance reached at the peak of the pulse. There is no possibility of moving focus if the initial condition at the edge of the nonlinear medium is a waist of the size of the observed filament.

B. The aerodynamic window

Aerodynamic windows were first developed in the 1970s as windows for very high power CO_2 lasers.[29] In an aerodynamic window, a supersonic flow of air is forced through a narrow nozzle. As the air flows through a curved expansion chamber, it creates a pressure gradient from vacuum to atmospheric pressure, which results in the effective separation of the low vacuum chamber (pressure of about 10 Torr) from the atmosphere.[29,30] The profile of the air channel cut in an aluminum block is shown in Fig. 3(a). The red arrow indicates the direction of propagation of light, entering from the right (vacuum side) through a hole or slit, and exiting at atmospheric pressure to the left. A setup for the investigation of the optical quality of the window is shown in Fig. 3(b). The pressure distribution in the expansion chamber of the aerodynamic window is shown by the color coded profile. The supersonic flow is generated by an air compressor providing a flow of up to 10 m^3/min at a pressure of 8 kg/cm^2. The aerodynamic window provides a high damage threshold barrier between the atmosphere and the vacuum chamber, enabling linear propagation of the intense pulse up to the boundary of the nonlinear medium (air in this case).

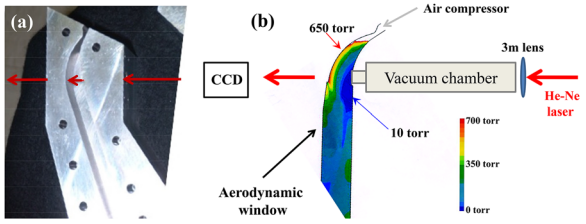

FIG. 3. (a) Profile of the aerodynamic window nozzle and expansion chamber, cut in an aluminum block. The cut is 20 mm deep. The arrows indicate the direction of propagation of the light from vacuum to the atmosphere. The light passes through a 3 mm diameter hole or, in another realization, a 3 × 20 mm^2 slot. (b) Setup for investigation of the stability of the beam profile of a He–Ne laser going through the aerodynamic window.

1. Beam pointing stability

The fact that a supersonic air flow is used to generate the pressure gradient in an aerodynamic window may raise a suspicion about the stability of a laser beam going through such a window. In order to address this issue, an expanded He–Ne laser focused with a 3 m lens is used to investigate the beam pointing stability through the aerodynamic window [Fig. 3(b)]. Successive images of the beam profile of the He–Ne laser are captured at 2.4 m from the exit point of the aerodynamic window by a high resolution camera and saved for further processing. We compare the centroid or the center of gravity ($\bar{x}$) and the beam size (w) mean square deviation (MSQ)[31,32] of the He–Ne laser in two cases of operational and non-operational aerodynamic window. All other conditions are kept the same. For the center of gravity along x,

$$\bar{x} = \frac{\sum_{i,j=0}^{N} x_i I(x_i, y_j)}{\sum_{i,j=0}^{N} I(x_i, y_j)},$$

while the beam waist along the x direction is defined as

$$w_x = \sqrt{\frac{\sum_{i,j=0}^{N} (x_i - \bar{x})^2 I(x_i, y_j)}{\sum_{i,j=0}^{N} I(x_i, y_j)}}.$$

These quantities are calculated and plotted in Fig. 4 for 48 successive images. Surprisingly, the fluctuations are reduced when the aerodynamic window is operating, indicating that the beam is more disturbed by the turbulence in the stagnant air of the 3 m tube than by the window. The calculated standard deviations of the datasets for the measurement of the centroid of the beam in the cases of operational vs non-operational aerodynamic window are 1.84 and 7.52 pixels, respectively (one pixel is 15 μm). In addition, the calculated standard deviations of the datasets for the measurement of the beam waist in the cases of operational vs non-operational aerodynamic window are 0.015 and 0.024 mm, respectively. Since all other conditions are the same, we can conclude that the stability of the laser beam going through the vacuum tube terminated by the operational aerodynamic window is improved and the beam profile has less fluctuations both in the location of its centroid and its beam waist.

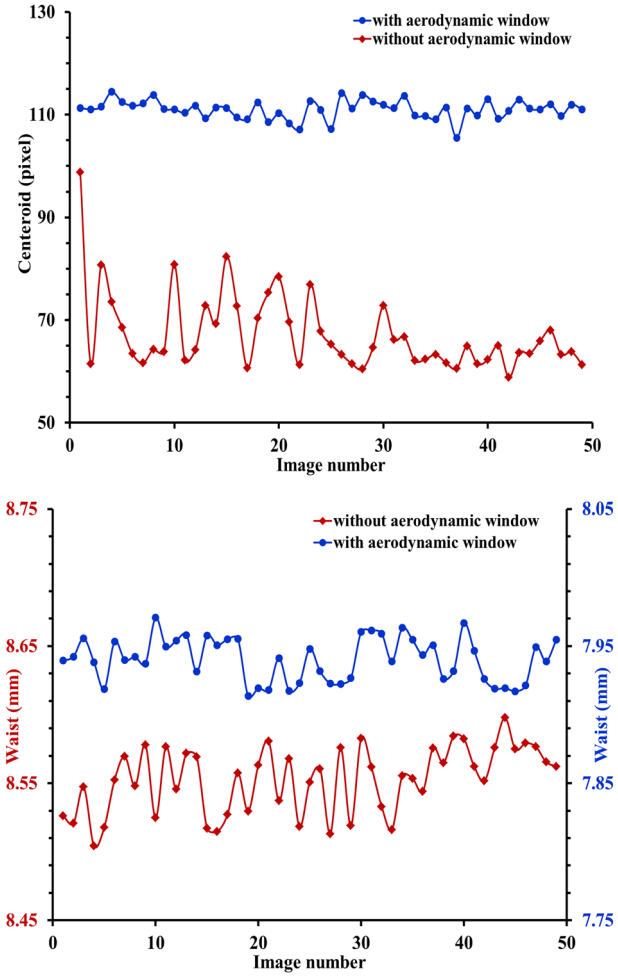

FIG. 4. Comparison between the centroid (top) and the beam waist (bottom) of the beam profile of a He–Ne laser (for 49 successive images), with and without aerodynamic window. The expanded He–Ne laser beam is focused with a 3 m lens.

IV. UV FILAMENT SPATIAL PROFILE MEASUREMENTS

It has been established that properties of filaments, such as length and plasma density, are dependent on the focusing conditions used for the initiation of the filament.[33,34] Thus, various lenses with focal lengths from 0.5 to 9 m have been used for filament experimental generation and detection. The results of the investigation of spatial profiles of the filaments generated by the 3 and 9 m lenses are presented in Subsections IV A and IV B.

Measuring the beam profile of a 300 mJ pulse of less than 200 ps in a sub-millimeter cross section is a challenge. The solution found to attenuate *linearly* the beam is to use a 15 cm diameter grazing incidence coated fused silica plate.[30] Because one linear dimension of the filament is stretched over 15 cm, the intensity can be kept below the damage threshold of the coating. A 355 nm coating at normal incidence is a standard coating for an excimer laser. The reflectivity of such a coating for s-polarization at eight different wavelengths close to 266 nm was measured to be $0.5 \cdot 10^{-6}$ (Fig. 5).

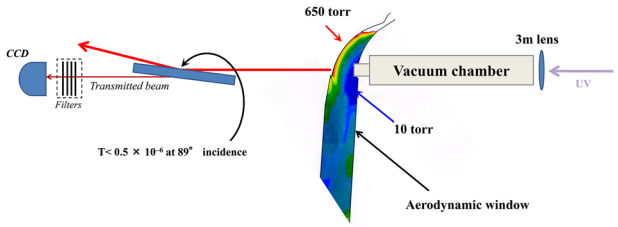

FIG. 5. Experimental setup used for observing the spatial profile of the UV filaments. The beam is linearly attenuated by a grazing incidence plate (BK7, 15 mm thickness, 150 mm diameter) coated for maximum reflectivity at 355 nm (normal incidence). The beam is thereafter further attenuated by neutral density filters before being recorded by a CCD.

A. 3 m lens

The spatial profiles of the UV filaments generated with a 3 m lens are compared for two different schemes of focusing in air and in vacuum (operational aerodynamic window). The distance between the 3 m lens and the entrance window of the vacuum chamber is chosen in a way that the geometrical focus is located a few millimeters before the exit of the aerodynamic window. As mentioned before, by using the aerodynamic window, it is possible to focus the UV pulse in vacuum before the onset of the UV filament, resulting in a different initial preparation phase for the filament.

In Figs. 6(a) and 6(b), the beam profile of the UV filament for the case of focusing in vacuum using a 3 m lens (operational aerodynamic window) is represented. The UV filament has a FWHM of about 375 μm, which is measured at the distance of 2 m from the exit of the aerodynamic window. A transverse image of a weak beam (sufficiently attenuated not to induce any nonlinear effect) is shown in Fig. 6(c). The 20 μm indicated on the figure corresponds to the beam size at the exit plane of the window, a few cm after the waist of w = 13 mm, hence the initial condition for the filamenting beam exiting the aerodynamic window at the end of the 3 m vacuum tube. The transverse image of the UV filament, which is taken using an image intensifier for the same experimental conditions, is shown in Fig. 6(d). It can be seen that the FWHM of the filament in this image is 300 μm, which is in good agreement with beam profile measurements. Figure 6 is another demonstration that the moving focus model[36] does not apply, even for these subnanosecond pulses. It is a rare example of a filament starting from a 13 μm waist to evolve into the quasi-steady state filament shown in Fig. 6(d).

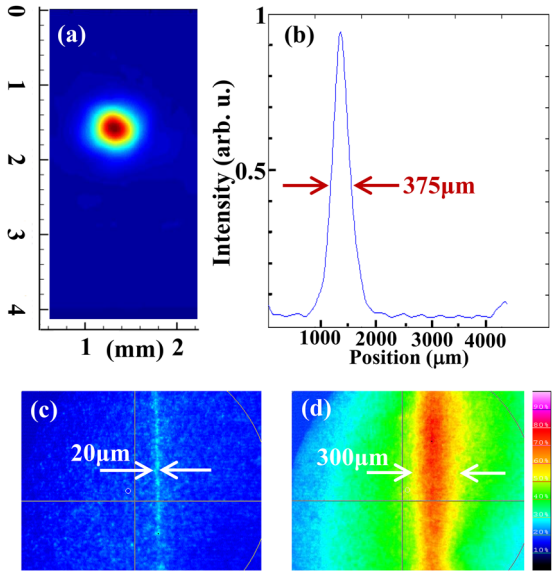

FIG. 6. (a) and (b) UV filament beam profile for the case of focusing with a 3 m lens in vacuum (operational aerodynamic window).[35] The UV filament has a FWHM of about 375 μm. This is measured using the setup described in Fig. 5. The CCD is 2 m away from the exit point of the aerodynamic window. (c) Calibration image of the focused UV laser beam at very low power, exiting the aerodynamic window, taken with an image intensifier and a CCD. The 13 μm waist is a few cm before the exit plane of the window. (d) Image of the filament taken with the image intensifier and a CCD, showing a FWHM of about 300 μm.

Filaments obtained by focusing in vacuum have smaller diameters compared to the ones obtained by direct focusing in air.[35,37] In the case of focusing in vacuum, diameters in the range of 300–400 μm have been measured for different distances up to 4 m with respect to the exit of the aerodynamic window. These distances are more than two orders of magnitude larger than the Rayleigh range. Similar measurements for the case of focusing in air resulted in a diameter of the order of 1 mm.[35] The probability of forming a filament is also reduced in the case of focusing in air, as compared to the case of focusing in vacuum. This is explained by the fact that the nonlinear losses during the initial self-focusing phase are prevented, and, as shown in Subsection III B 1, wavefront distortion by air turbulence is avoided in the 3 m vacuum tube. The measured beam profiles are in good agreement with the previous theoretical calculations.[19]

B. 9 m lens

The beam profiles are recorded without the use of the aerodynamic window, outside of the laboratory. The laser beam is sent through a periscope to a 9 m focusing lens at 30 m of the source. The multiple reflections account for an attenuation of about 30% in the energy of the beam. Figure 7 shows pictures of successive beam profiles as a function of the distance from the 9 m lens. The initially super-Gaussian profile has diffracted, propagated through turbulent air, until reaching the 9 m focal lens (beam diameter 20 cm). Multiple filaments are generated, as reported in similar focusing conditions (f = 10 m) with near-infrared filaments.[38] The distance over which the filaments are observed is about 2 m, which is much longer than the Rayleigh range (~1 mm) for this focusing scheme.

V. SHADOWGRAPHS OF UV FILAMENTS

Sudden heating of a gas with a high intensity laser (a UV filament in the present case) will create a low density plasma channel. The impulsive heating of a gas creates shock-waves of cylindrical symmetry, which propagate outward from the center line, leaving the low density channel behind.[39] Initially, the shock-waves propagate with velocities much larger than the speed of sound, i.e., supersonic, but their velocity rapidly decreases to the speed of sound as they propagate. The diameter of the low density tube is determined by the deposited energy and the gas pressure.[40,41]

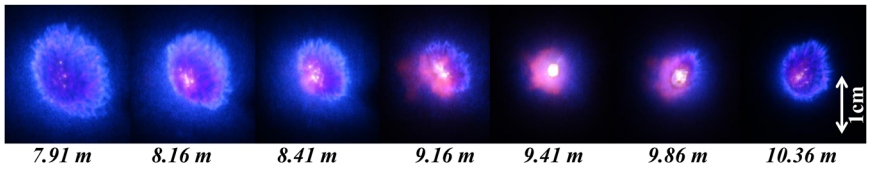

FIG. 7. The beam profiles of UV filaments at different distances from the 9 m focusing lens. These beam profiles are captured by a digital camera recording the impact of the UV filament on a piece of paper. Different colors correspond to the fluorescent emission from the paper, which is changing based on the impacted beam intensity. The white dots in the figure are related to multiple filaments.

Shadowgraphy is an optical technique, which can be used for the investigation of small amplitude changes in the refractive index in transparent materials, which in the case of UV filaments is a consequence of the change in the air density.[42] The shadowgraphy technique is used to investigate the characteristics of the mentioned low density tube and shock-waves created by the UV filaments. The probe beam is a collimated and expanded (about 6 cm) green (532 nm) pulse with 10 ns temporal pulse width. This probe beam is sent perpendicular to the UV filament and is imaging the area of interest on a screen located in a 1 m distance from the filament (Fig. 8).

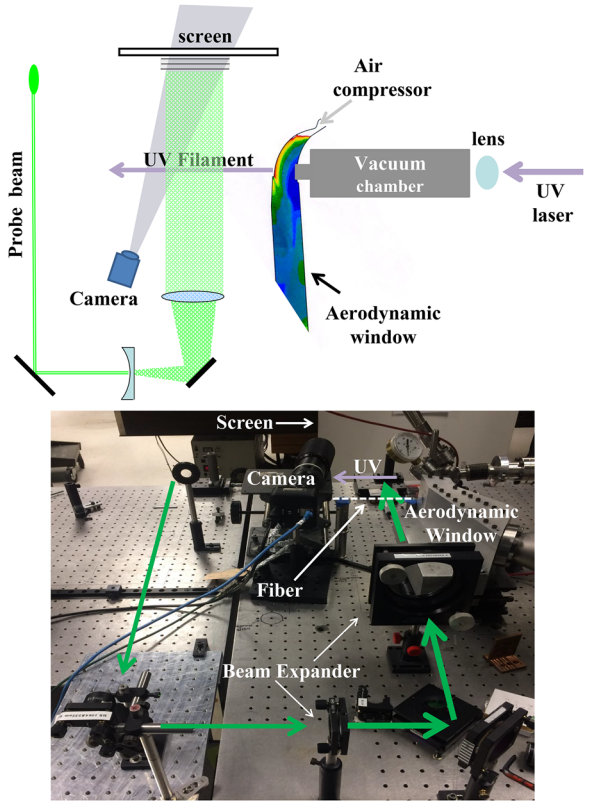

FIG. 8. Top: schematic diagram of the shadowgraphy setup. Bottom: picture of the shadowgraphy setup.

A CCD camera is used to capture the shadowgrams on the screen. An optical fiber is placed just below the UV filament, providing a reference for the size of shadowgrams. A master-clock is used to synchronize the UV laser, the green laser, and the camera. A delay generator controls the relative delay time between the probe beam and the UV laser, making it possible to investigate the temporal evolution of the shock-waves and the low density channel.

The shadowgrams of UV filaments in different focusing schemes were investigated. The results of focusing with 1 and 3 m lenses are presented here. In Fig. 9, selected shadowgrams of UV filaments are displayed for different time delays between the UV laser and the probe beam for 1 m focusing. From the shadowgrams, we can conclude that, as expected, the filament length is longer when focusing with a 3 m lens. In this case, the low density tube is present all over the probe beam. This fact is also evident from Fig. 10, which is a direct image of the plasma channel of the filament taken with a digital camera. The shock-waves created from tighter focusing are more intense. This is also expected, since in tighter focusing higher plasma electron densities are created. The higher intensity deposited by the filament[43,44] affects the width of the low density tube. The

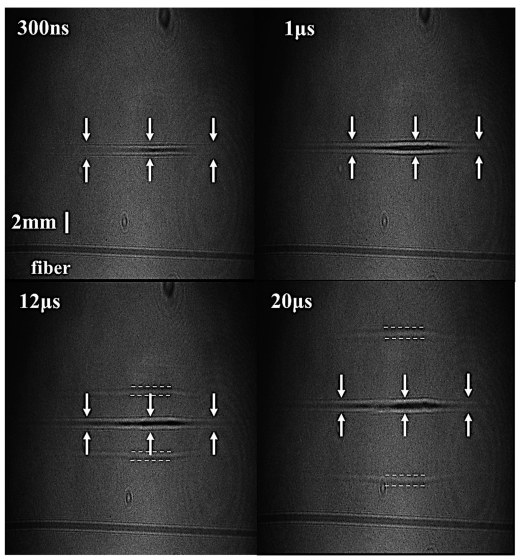

FIG. 9. Shadowgraphs of the UV filament vs time focused with a 1 m lens. The low density tube and shock-waves are demonstrated by white arrows and dashed lines, respectively.

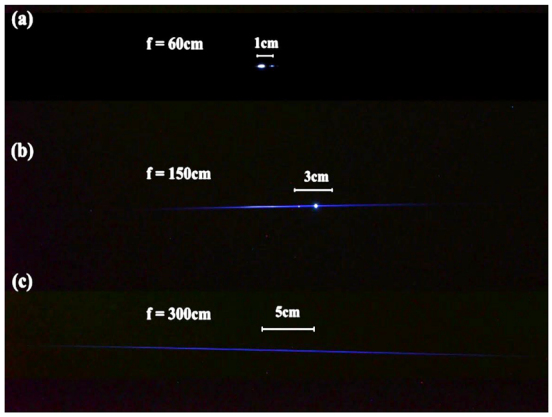

FIG. 10. Image of the plasma channels taken with a digital camera from the side for the filaments generated with three focusing lenses of (a) 0.6 m, (b) 1 m, and (c) 3 m.[37] The beam diameter is the same for all three pictures. The Rayleigh range is ~1 mm for (c), hence much smaller than the plasma length.

widths of the low density channels in both cases are measured using the image of the fiber as reference. These widths are 485 and 420 μm for the 3 and 1 m lenses, respectively. The values mentioned are measured at the delay of 12 μs with respect to the UV laser. However, it should be mentioned that after the initiation phase, as the shock-wave propagates outward (Fig. 11), the remaining low density channel will have approximately the same width as long as it is sustained. The widths of these channels are in agreement with the UV filament FWHM reported in Sec. IV. The shock-waves propagate initially with supersonic velocities, but their velocity rapidly decreases to the speed of sound, in good agreement with our measurements of the speed of shock-waves shown in Fig. 11.

Another observation from the shadowgraphy data is that the generated waveguide is formed within 300 ns and remains stable and uniform up to approximately 200 μs. As a result, at a repetition rate above 5 kHz, a series of ionizing laser pulses will lead to the

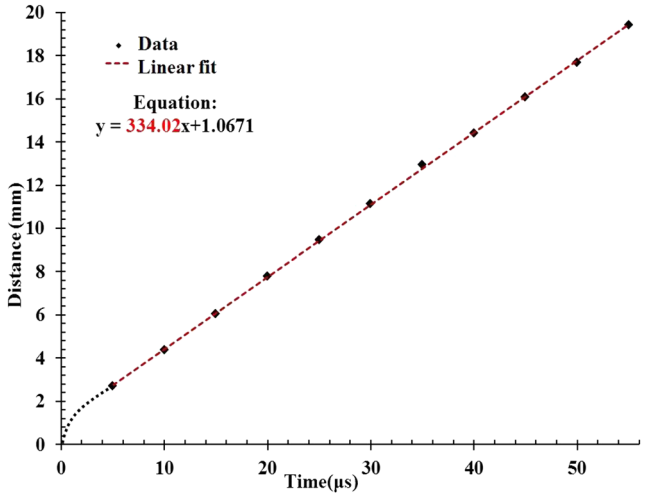

FIG. 11. Shock-wave propagation vs time for shock-waves generated by UV filaments with a 1 m lens.

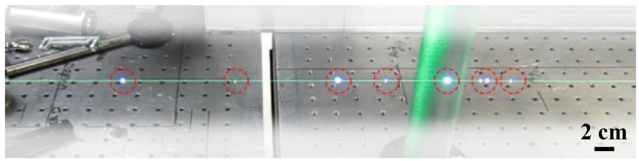

FIG. 12. Picture of the Rayleigh scattering and plasma beads generated by a 532 nm, 1.2 J pulse of 200 ps duration. The plasma beads are indicated by red circles (from Ref. 37).

production of heat bursts, and each heat burst will create a shock-wave that does not decay before the arrival of the next pulse. The generation of this waveguide based on the shock-wave being long lived can possibly result in a stationary waveguide.

Since our source produces 1.2 J pulses of 200 ps duration at 532 nm, an attempt was made to create filaments with a 3 m focal distance lens. The appearance of plasma beads in Fig. 12 suggests that the 200 ps pulses are too long at that wavelength to prevent avalanche breakdown.

VI. APPLICATIONS OF FILAMENT PRODUCED SHOCK-WAVES

A. Guiding

The stationary waveguides mentioned in Sec. V can be used for optical guiding of another filamenting laser pulse.[45–48] This can have possible applications for remote sensing,[1–3] directed energy applications,[49,50] and triggering and guiding of electrical discharges.[4–8]

In Ref. 45, the authors have investigated waveguides generated by fs IR filaments. Their experiments in the single filament scenario have shown that an initial density hole will grow for tens of nanoseconds as a shock-wave propagates outward. Later, after approximately 1–2 μs, the pressure inside the waveguide reaches equilibrium. This generated leaky waveguide will decay in ms time scales. These and also measurements reported in Ref. 39 are in agreement with our shadowgraphy study using UV filaments reported in Sec. V. Positive index profiles—hence dielectric waveguides—were achieved with multiple IR filaments forming a symmetric four-lobed pattern, which created a long-lived, of the order of ms, waveguide in air. It was also reported that the length of these waveguides depended only on the propagation distance of the inducing fs array of filaments.[45] A probe laser beam used to investigate the guiding property of the positive pressure waveguide indicated a peak guiding efficiency of 70% at ≃600 μs, which decreased to 15% at ≃2 ms. In their latest publication,[46] the authors reported successful guiding over lengths of up to 30 cm.

In applications to remote sensing, the generated waveguide can not only be used for guiding a second high peak power filament to irradiate a sample, but it has also been shown that these air waveguides can act as a broadband collection optics that enhances the returning signal from the sample, which will improve the sensitivity in remote sensing.[47] Application of UV filaments for remote sensing is discussed in more detail in Subsection VI B.

B. Remote sensing

Another application of UV filaments is high resolution remote sensing at atmospheric pressures via Laser Induced Breakdown

Spectroscopy (LIBS). This technique attempts to gain information on the irradiated material through the spectrum it emits upon impact by the laser pulse. This emission spectrum is pressure and Stark broadened, and it has to be corrected for Stark shift in order to identify the emission lines. This Stark shift leads to unwanted errors[51,52] in the analysis of the composition of a sample through the emission spectrum. There are structures within the emission line—essentially dips—which have been dismissed as an annoyance.[51,53] Considerable effort has been made to eliminate them either through experimental techniques or through simulation and data analysis.[54–56] These dips are mostly observed in the spectrum delayed by typically 5 μs or more. In the case of irradiation by UV filaments, they are much more pronounced and appear almost immediately after irradiation.[3] In contrast to the emission, the dips are centered from the early times exactly at the tabulated frequency of the corresponding atomic transition. They are interpreted as re-absorption by the material ejected upon impact from the filament. Contrary to the Lorentz broadened emission line (indicating pressure and Stark broadening), the re-absorption dip fits a Gaussian shape and is considerably narrower. Relying on the absorption dip results in a higher resolution, making even isotopic selective LIBS possible[3,57,58] at atmospheric pressures. An example of LIBS spectrum of a uranium sample irradiated by a UV filament at atmospheric pressures is shown in Fig. 13. A resolution of about 9 pm for the self-absorption dip is observed, while the emission line has a FWHM of about 124 pm.

Even in the case of very light atoms, such as lithium, in which the emission lines are really broad (≃3 nm FWHM), it is possible, using the self-absorption dip, to resolve the isotopic shift between the two natural stable isotopes of Li.[57] In Fig. 14, LIBS spectra of these two isotopes are presented. The transition lines for these two isotopes are at 670.830 nm (Li7) and 670.849 nm (Li6), which indicates an isotopic shift of 19 pm. It can be seen that the self-absorption

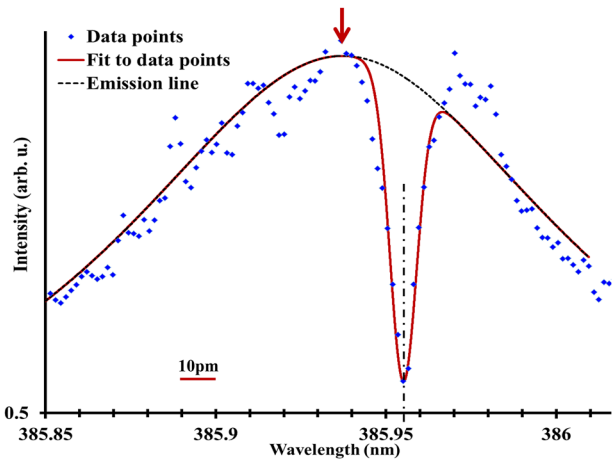

FIG. 13. LIBS spectrum of the uranium line at 385.957 nm. The sample was irradiated by a UV filament at atmospheric pressure. The solid red line is the Lorentzian–Gaussian fit to the data. The dashed black line is the Lorentzian fit, which represents the emission line. The vertical arrow points to the Stark shifted peak of the Lorentzian fitted emission line. The dotted-dashed black vertical line shows the center of the re-absorption dip, emphasizing the absence of Stark shift in the absorption feature.

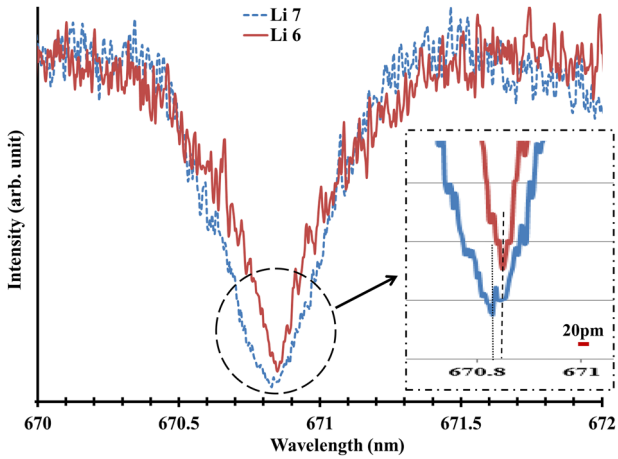

FIG. 14. LIBS spectra of the two isotopes of lithium. The transition lines for these two isotopes are at 670.830 nm (Li7) and 670.849 nm (Li6), which indicates an isotopic shift of 19 pm. The emission line extends far beyond the boundaries of the figure.

dip of lithium has a FWHM of about 0.3 nm and is not affected by the Stark effect. By using the self-absorption dip, it was possible to resolve this isotopic shift. In addition, in Ref. 3, it is demonstrated that by using the self-absorption dip, it is possible to resolve the two lines of chromium at 301.491 and 301.476 nm that are 15 pm apart. It is worth mentioning that from these results, it can be concluded that the 25 pm isotopic shift between the two isotopes of uranium can be resolved by utilizing the self-absorption dip.

In LIBS, immediately after the filament/laser impacts the sample, a plume is generated. As this plume expands, an outward propagating shock-wave is formed that will leave behind a bubble. Using the same shadowgraphy technique as in Sec. V, we have investigated this shock-wave and the bubble. In Fig. 15, the shadowgraphs of the plume and the propagating shock-wave for different delay times with respect to the impact time can be seen. In this set of experiments, the target is a piece of aluminum and the UV pulse energy of 300 mJ. The FWHM of the self-absorption dip was 20 pm. Self-absorption occurs as the emitted light from the excited atoms at the center of the bubble is absorbed by the atoms in the ground state at the outer layers of the bubble. These outer layers of the bubble happen to have lower densities. The fact that these atoms are at the ground level and have lower density is the reason that the self-absorption dip has a much narrower FWHM as the collisional and Stark broadening mechanisms are suppressed. This also results in the absence of any Stark related red shift in the self-absorption dip.[3]

C. Drag reduction for supersonic aircrafts

A contribution to the understanding of the thermodynamics associated with filaments can be found in a proposal for a futuristic application of filamentation to hypersonic flights.[59] In a new race for hypersonic fighter jets, there have been attempts to use plasma for reducing the drag of solids in supersonic flow, most often using electrodes to create a plasma.[60–62] This implies putting a solid object in front of a wing's leading edge of which the drag should be reduced, hence adding another drag. In Ref. 59, the authors proposed to use

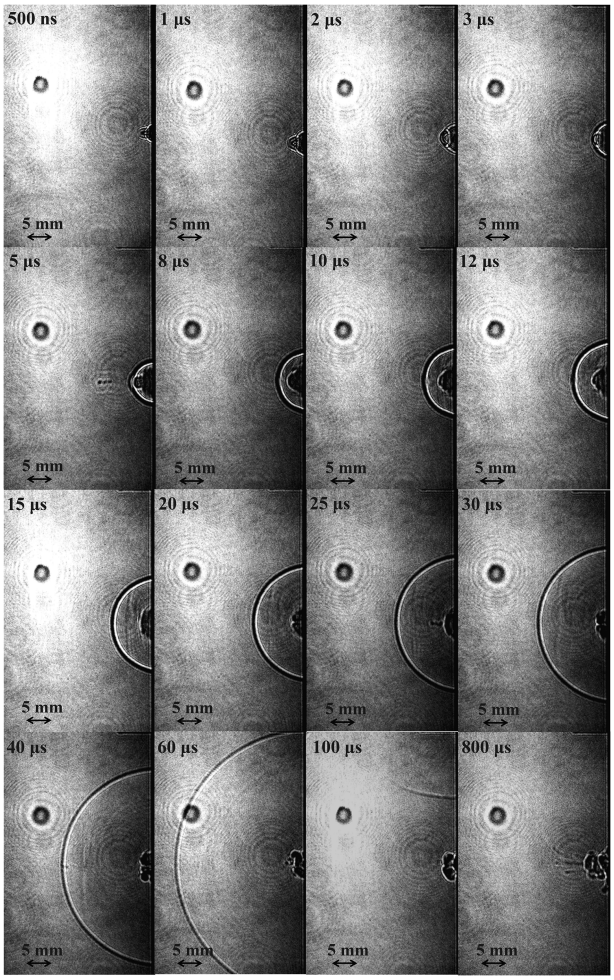

FIG. 15. Shadowgraphy of the plume in LIBS experiment for various delay times. The target is a piece of aluminum, and the UV pulse energy is 300 mJ. The self-absorption dip has a FWHM of 20 pm. The dark spot, appearing in all the images, is the defect of the CCD.

filaments to achieve an electrode-less approach. The demonstration involved a Mach 3 supersonic wind tunnel in which a test model mounted on a balance measuring the axial component of the drag was inserted. The test model was a blunted cone 60 mm diameter, with piezoelectric transducers on the side to monitor the pressure at the upper and lower parts of the model. An 800 nm filament produced by a femtosecond terawatt laser was sent upstream to the air flow through a 3 mm hole at the center of the cone. A 50% transient drag reduction is measured with the balance on which the model is mounted.

What makes this experiment relevant to the topic of hydrodynamic waveguiding with filaments is the surprising similarity of the observation with those of the laser impact produced shock-wave presented in Subsection VI B. In both cases, there is a "bubble" of lower density gas in front of the solid, due in part to the hot channel and the axial pressure gradient of the shock front. However, while in LIBS, the shock-wave is produced by the ejection of material from the solid surface, in the drag reduction experiment the shock-wave due to the impact of the supersonic jet on the solid is interacting with that of the filament. A low density region in LIBS is responsible for the very narrow re-absorption lines. A low density region hugging the solid test model is responsible for the reduced drag in the supersonic experiment. In both cases, the low density region persists for $\approx 100\ \mu s$.

Of particular interest for future studies of the waveguiding properties of the filament wake are the tools used to analyze the properties of the bubble. Schlieren pictures made by transverse illumination with a 50 ns diode laser at 630 nm exhibited a better contrast than shadowgraphy. Quantitative data on the 2D transverse profile of the index of refraction were obtained through an Abel-inversion algorithm of four-wave shearing interferometry.

These experiments seem also to suggest that the waveguiding may be possible at sea level, but also at high altitude. The experiments in Ref. 59 have been performed at gas densities typical of a supersonic flight at altitudes between 6 and 15 km (equivalent pressure at room temperature between 200 and 550 mbar). They obtained filaments at pressure as low as 100 mbar.

ACKNOWLEDGMENTS

This work was supported by the Army Research Office (ARO; Grant No. W911NF-19-1-0272) and the U.S. Department of Energy (DOE; Grant No. DESC0011446).

DATA AVAILABILITY

The data that support the findings of this study are available from the corresponding author upon reasonable request.

REFERENCES

[1] M. Baudelet, M. Boueri, J. Yu, S. S. Mao, V. Piscitelli, X. Mao, and R. E. Russo, "Time-resolved ultraviolet laser-induced breakdown spectroscopy for organic material analysis," Spectrochim. Acta, Part B **62**, 1329–1334 (2007), a Collection of Papers Presented at the 4th International Conference on Laser Induced Plasma Spectroscopy and Applications (LIBS 2006).

[2] K. Stelmaszczyk, P. Rohwetter, G. Méjean, J. Yu, E. Salmon, J. Kasparian, R. Ackermann, J.-P. Wolf, and L. Wöste, "Long-distance remote laser-induced breakdown spectroscopy using filamentation in air," Appl. Phys. Lett. **85**, 3977–3979 (2004).

[3] A. Rastegari, M. Lenzner, J.-C. Diels, K. Peterson, and L. Arissian, "High resolution remote spectroscopy and plasma dynamics induced with UV filaments," Opt. Lett. **44**, 147–150 (2019).

[4] T. Produit, P. Walch, C. Herkommer, A. Mostajabi, M. Moret, U. Andral, A. Sunjerga, M. Azadifar, Y.-B. André, B. Mahieu, W. Haas, B. Esmiller, G. Fournier, P. Krötz, T. Metzger, K. Michel, A. Mysyrowicz, M. Rubinstein, F. Rachidi, J. Kasparian, J.-P. Wolf, and A. Houard, "The laser lightning rod project," Eur. Phys. J. Appl. Phys. **93**, 010504 (2021).

[5] F. Théberge, J.-F. Daigle, J.-C. Kieffer, F. Vidal, and M. Châteauneuf, "Laser-guided energetic discharges over large air gaps by electric-field enhanced plasma filaments," Sci. Rep. **7**, 040063 (2017).

[6] A. Rastegari, E. Schubert, C. Feng, D. Mongin, B. Kamer, J. Kasparian, J.-P. Wolf, L. Arissian, and J.-C. Diels, "Beam control through nonlinear propagation in air and laser induced discharges," in *Laser resonators and beam control XVIII, Photonics West, Conference* (SPIE, San Francisco, CA, 2016), pp. 9727–9751.

[7] E. Schubert, A. Rastegari, C. Feng, D. Mongin, B. Kamer, J. Kasparian, J.-P. Wolf, L. Arissian, and J.-C. Diels, "HV discharge acceleration by sequences of UV laser filaments with visible and near-infrared pulses," New J. Phys. **19**, 123040 (2017).

[8]A. Houard, C. D'Amico, Y. Liu, Y. B. Andre, M. Franco, B. Prade, A. Mysyrowicz, E. Salmon, P. Pierlot, and L.-M. Cleon, "High current permanent discharges in air induced by femtosecond laser filamentation," Appl. Phys. Lett. **90**, 171501 (2007).
[9]Q. Luo, W. Liu, and S. L. Chin, "Lasing action in air induced by ultra-fast laser filamentation," Appl. Phys. B **76**, 337–340 (2003).
[10]L. Arissian, B. Kamer, A. Rastegari, D. Villeneuve, and J.-C. Diels, "Transient gain from N_2^+ in light filaments," Phys. Rev. A **98**, 053438 (2018).
[11]M. Britton, M. Lytova, P. Laferriare, P. Peng, F. Morales, D. H. Ko, M. Richter, P. Polynkin, D. M. Villeneuve, C. Zhang, M. Ivanov, M. Spanner, L. Arissian, and P. B. Corkum, "Short- and long term gain dynamics in N_2^+ air lasing," Phys. Rev. A **100**, 013406 (2019).
[12]A. Mysyrowicz, R. Danylo, A. Houard, V. Tikhonchuk, X. Zhang, Z. Fan, Q. Liang, S. Zhuang, L. Yuan, and Y. Liu, "Lasing without population inversion in N_2^+," APL Photonics **4**, 110807 (2019).
[13]A. Rastegari, J.-C. Diels, L. R. Liu, and L. Arissian, "Measurement of delayed fluorescence in N_2^+ with streak camera," arXiv:2001.00437 (2020).
[14]S. A. Akhmanov, A. P. Sukhorukov, and R. V. Khokhlov, "Self focusing and self trapping of intense light beams in a nonlinear medium," Sov. Phys. JETP **23**, 1025–1033 (1966).
[15]E. Freysz, M. Afifi, A. Ducasse, B. Pouligny, and J. R. Lalanne, "Giang optical non-linearities of critical micro-emulsions," J. Phys. Lett. **46**, 181–187 (1985).
[16]R. Y. Chiao, E. Garmire, and C. H. Townes, "Self-trapping of optical beams," Phys. Rev. Let. **13**, 479–482 (1964).
[17]J. H. Marburger, "Self-focusing," in *Progress in Quantum Electronics*, edited by J. H. Sanders and S. Stendholm (Pergamon, Oxford, 1977), Vol. 4, pp. 35–110.
[18]A. Braun, G. Korn, X. Liu, D. Du, J. Squier, and G. Mourou, "Self-channeling of high-peak-power femtosecond laser pulses in air," Opt. Lett. **20**, 73–75 (1995).
[19]O. Chalus, A. Sukhinin, A. Aceves, and J.-C. Diels, "Propagation of non-diffracting intense ultraviolet beams," Opt. Commun. **281**, 3356–3360 (2008).
[20]X. M. Zhao, P. Rambo, and J.-C. Diels, "Filamentation of femtosecond UV pulses in air," in *QELS* (Optical Society of America, Baltimore, MA, 1995), Vol. 16, p. 178 (QThD2).
[21]J. Schwarz, P. Rambo, J.-C. Diels, M. Kolesik, E. M. Wright, and J. V. Moloney, "UV filamentation in air," Opt. Commun. **180**, 383–390 (2000).
[22]X. Xu and J.-C. Diels, "Stable single-axial-mode operation of injection-seeded Q-switched Nd:YAG laser by real-time resonance tracking method," Appl. Phys. B **114**, 579 (2014).
[23]X. Xu, "High power UV source development and its applications," Ph.D. thesis, The University of New Mexico, Albuquerque, NM, 2015.
[24]X. Xu, C. Feng, and J.-C. Diels, "Optimizing sub-ns pulse compression for high energy application," Opt. Express **22**, 13904–13915 (2014).
[25]C. Feng, X. Xu, and J.-C. Diels, "High-energy sub-phonon lifetime pulse compression based on stimulated Brillouin scattering in liquids," Opt. Express **25**, 12421–12434 (2017).
[26]C. Feng, X. Xu, and J.-C. Diels, "Generation of 300 ps laser pulse with 1.2 J energy by stimulated Brillouin scattering in water at 532 nm," Opt. Lett. **39**, 3367–3370 (2014).
[27]T. D. Grow, A. A. Ishaaya, L. T. Vuong, A. L. Gaeta, N. Gavish, and G. Fibich, "Collapse dynamics of super-Gaussian beams," Opt. Express **14**, 5468–5475 (2006).
[28]Y. R. Shen and M. M. T. Loy, "Theoretical interpretation of small-scale filaments of light originating from moving focal spots," Phys. Rev. A **3**, 2099–2105 (1971).
[29]E. M. Parmentier and R. A. Greenberg, "Supersonic flow aerodynamic windows for high-power lasers," AIAA J. **11**, 943–949 (1973).
[30]J.-C. Diels, J. Yeak, D. Mirell, R. Fuentes, S. Rostami, D. Faccio, and P. di Trapani, "Air filaments and vacuum," Laser Phys. **20**, 1101–1106 (2010).
[31]T. S. Ross, *Laser Beam Quality Metrics* (SPIE, 2013).
[32]Y. Du, Y. Fu, and C. Zheng, "Beam quality M^2 factor matrix for non-circular symmetric laser beams," Laser Phys. **27**, 025001 (2016).
[33]K. Lim, M. Durand, M. Baudelet, and M. Richardson, "Transition from linear- to nonlinear-focusing regime in filamentation," Sci. Rep. **4**, 7217 (2014).
[34]F. Théberge, W. Liu, P. T. Simard, A. Becker, and S. L. Chin, "Plasma density inside a femtosecond laser filament in air: Strong dependence on external focusing," Phys. Rev. E **74**, 036406 (2006).
[35]O. Chalus, Study of Nonlinear Effects of Intense UV Beams in the Atmosphere, Ph.D. thesis, University of New Mexico and University Louis Pasteur, Strasbourg, 2007.
[36]A. Brodeur, C. Y. Chien, F. A. Ilkov, S. L. Chin, O. G. Kosareva, and V. P. Kandidov, "Moving focus in the propagation of ultrashort laser pulses in air," Opt. Lett. **22**, 304–306 (1997).
[37]C. Feng, "Sub-nanosecond UV filaments and their applications for remote spectroscopy and high-voltage discharges," Ph.D. thesis, University of New Mexico, Albuquerque, NM, 2016.
[38]T. Fujii, M. Miki, N. Goto, A. Zhidkov, T. Fukuchi, Y. Oishi, and K. Nemoto, "Leader effects on femtosecond-laser-filament-triggered discharges," Phys. Plasmas **15**, 013107 (2008).
[39]Y.-H. Cheng, J. K. Wahlstrand, N. Jhajj, and H. M. Milchberg, "The effect of long timescale gas dynamics on femtosecond filamentation," Opt. Express **21**, 4740 (2013).
[40]M. N. Plooster, "Shock waves from line sources. Numerical solutions and experimental measurements," Phys. Fluids **13**, 2665–2675 (1970).
[41]K. Kremeyer, K. Sebastian, and C.-W. Shu, "Computational study of shock mitigation and drag reduction by pulsed energy lines," AIAA J. **44**, 1720–1731 (2006).
[42]P. K. Panigrahi and K. Muralidharl, "Laser schlieren and shadowgraph," in *Schlieren and Shadowgraph Methods in Heat and Mass transfer* (Springer, 2012), Chap. II.
[43]X.-L. Liu, X. Lu, X. Liu, T.-T. Xi, F. Liu, J.-L. Ma, and J. Zhang, "Tightly focused femtosecond laser pulse in air: From filamentation to breakdown," Opt. Express **18**, 26007–26017 (2010).
[44]F. V. Potemkin, E. I. Mareev, A. A. Podshivalov, and V. M. Gordienko, "Laser control of filament-induced shock wave in water," Laser Phys. Lett. **11**, 106001 (2014).
[45]N. Jhajj, E. Rosenthal, R. Birnbaum, J. K. Wahlstrand, and H. M. Milchberg, "Demonstration of long-lived high-power optical waveguides in air," Phys. Rev. X **4**, 011027 (2014).
[46]B. Miao, L. Feder, J. E. Shrock, A. Goffin, and H. M. Milchberg, "Optical guiding in meter-scale plasma waveguides," Phys. Rev. Lett. **125**, 074801 (2020).
[47]E. W. Rosenthal, N. Jhajj, J. K. Wahlstrand, and H. M. Milchberg, "Collection of remote optical signals by air waveguides," Optica **1**, 5–9 (2014).
[48]O. Lahav, L. Levi, I. Orr, R. A. Nemirovsky, J. Nemirovsky, I. Kaminer, M. Segev, and O. Cohen, "Long-lived waveguides and sound-wave generation by laser filamentation," Phys. Rev. A **90**, 021801 (2014).
[49]P. Sprangle, J. Penano, and B. Hafizi, "Optimum wavelength and power for efficient laser propagation in various atmospheric environments," J. Dir. Energy **2**, 71–95 (2006), https://www.deps.org/DEPSpages/JDE/JV2N1P5-Sprangle.pdf.
[50]P. Sprangle, B. Hafizi, A. Ting, and R. Fischer, "High-power lasers for directed-energy applications," Appl. Opt. **54**, F201–F209 (2015).
[51]D. A. Cremers and L. J. Radziemski, *Handbook of Laser-Induced Breakdown Spectroscopy* (Wiley, 2013).
[52]W. Hübert and G. Ankerhold, "Elemental misinterpretation in automated analysis of LIBS spectra," Anal. Bioanal. Chem. **400**, 3273–3278 (2011).
[53]F. Bredice, F. O. Borges, H. Sobral, M. Villagran-Muniz, H. O. Di Rocco, G. Cristoforetti, S. Legnaioli, V. Palleschi, L. Pardini, A. Salvetti, and E. Tognoni, "Evaluation of self-absorption of manganese emission lines in laser induced breakdown spectroscopy measurements," Spectrochim. Acta **61**, 1294–1303 (2006).
[54]J.-M. Li, L.-B. Guo, C.-M. Li, N. Zhao, X.-Y. Yang, Z.-Q. Hao, X.-Y. Li, X.-Y. Zeng, and Y.-F. Lu, "Self-absorption reduction in laser-induced breakdown spectroscopy using laser-stimulated absorption," Opt. Lett. **40**, 5224–5226 (2015).
[55]J. Hou, L. Zhang, W. Yin, S. Yao, Y. Zhao, W. Ma, L. Dong, L. Xiao, and S. Jia, "Development and performance evaluation of self-absorption-free laser-induced breakdown spectroscopy for directly capturing optically thin spectral line and realizing accurate chemical composition measurements," Opt. Express **25**, 23024–23034 (2017).
[56]H. Amamou, A. Bois, B. Ferhat, R. Redon, B. Rossetto, and M. Ripert, "Correction of the self-absorption for reversed spectral lines: Application to two

resonance lines of neutral aluminium," J. Quant. Spectrosc. Radiat. Transfer **77**, 365–372 (2003).
[57]A. Rastegari, M. Lenzner, C. Feng, L. Arissian, J.-C. Diels, and K. Peterson, "Exploiting shock wave and self-absorption for high resolution laser induced breakdown spectroscopy," in *CLEO: 2017* (Optical Society of America, San Jose, CA, 2017), p. JW2A.77.
[58]A. Rastegari, M. Lenzner, L. Arissian, J.-C. Diels, and K. Peterson, "Utilization of self-absorption for high resolution laser induced breakdown spectroscopy," in *CLEO: 2018* (Optical Society of America, San Jose, CA, 2018), p. SM1O.7.
[59]P. Q. Elias, N. Severac, J. M. Luyssen, Y. B. André, I. Doudet, B. Wattellier, J. P. Tobeli, S. Albert, B. Mahieu, R. Bur, A. Mysyrowicz, and A. Houard, "Improving supersonic flights with femtosecond laser filamentation," Sci. Adv. **4**, eaau5239 (2018).
[60]V. M. Fomin, P. K. Tretyakov, and J.-P. Taran, "Flow control using various plasma and aerodynamic appro," Aerosp. Sci. Technol. **8**, 411–421 (2004).
[61]E. Schülein, A. Zheltovodov, E. Pimonov, and M. Loginov, "Experimental and numerical investigation of electric-arc air spikles for blunt and sharp bodies at Mach 5," in *International Conference on Methods of Aerophysical Research* (ICMAR, 2008).
[62]V. L. Bychkov, L. P. Grachev, I. I. Esakov, A. A. Ravaev, and K. V. Khodataev, "Longitudinal DC electric discharge in a supersonic air flow," Tech. Phys. **49**, 833–838 (2004).